Unified series solution for the anti-plane effective magnetoelectroelastic moduli of three-phase fiber composites

P. Yan [a], C.P. Jiang [a,b,*], F. Song [b]

[a] School of Aeronautic Science and Engineering, Beijing University of Aeronautics and Astronautics, 100191 Beijing, China
[b] State Key Laboratory of Nonlinear Mechanics (LNM), Institute of Mechanics, Chinese Academy of Sciences, 100190 Beijing, China

ABSTRACT

The anti-plane magnetoelectroelastic behavior of three-phase magnetoelectroelastic composites (fiber/interphase/matrix) with doubly periodic microstructures is dealt with. With the aid of the matrix notation, the anti-plane magnetoelectroelastic coupling problem is formulated as same as the anti-plane piezoelectric coupling problem. And then the eigenfunction expansion-variational method (EEVM) is extended to solve such a problem. Series solutions for the effective magnetoelectroelastic moduli are presented, which are in a unified form for generally periodic fiber arrays, different unit cell shapes as well as different constituent properties, and are applicable for high volume fraction of fibers. With the present solution, it is found that the effective magnetoelectric coefficient of a two-phase composite may have two local extrema rather than only one extremum predicted by the Mori-Tanaka method. By optimizing the volume fraction, permutation and the choice of the constituent phases, the maximum magnitude of the effective magnetoelectric coefficient of a three-phase composite can be much larger than that of any of the two-phase composites, and the sign of the magnetoelectric coefficient can be changed, which is not observed in a two-phase composite. For composites with a generally periodic array of fibers, the effective magnetoelectric moduli can be anisotropic.

© 2012 Elsevier Ltd. All rights reserved.

1. Introduction

Magnetoelectric effect provides a useful tool for the conversion of energy between magnetic and electric forms. As a successful case of the man-made materials, magnetoelectroelastic composites can exhibit a magnetoelectric effect that is absent in each of the phases, by combining the piezoelectric effect in a piezoelectric phase and the piezomagnetic effect in a piezomagnetic phase. This kind of magnetoelectric effect in magnetoelectroelastic composites is caused by "product properties" (Van Suchtelen, 1972): the electric field and the magnetic field are related through the elastic strain. In a two-phase magnetoelectroelastic composite BaTiO₃/CoFe₂O₄, the magnetoelectric coefficient can be two orders of magnitude larger than that of the single-phase magnetoelectric materials (Van Run et al., 1974). Moreover, such a magnetoelectric effect in the composite can be observed at room temperature, whereas the magnetoelectric effect in single-phase magnetoelectric materials is often observed only at very low temperature

(Spaldin and Fiebig, 2005). Due to such outstanding performances, magnetoelectroelastic composites are increasingly applied in intelligent structures and smart devices (Ma et al., 2011; Nan et al., 2008; Pyu et al., 2002; Ramesh and Spaldin, 2007; Srinivasan, 2010). Motivated by such a finding, various designs of novel magnetoelectroelastic composites are presented, as well as the corresponding theoretical models and fabrication methods are developed (Eerenstein et al., 2006; Nan et al., 2008; Ramesh and Spaldin, 2007; Spaldin and Fiebig, 2005; Srinivasan, 2010).

According to the microstructural connectivity, the magnetoelectroelastic composites are generally categorized into particle composites, fiber composites, laminate composites, and so on (Nan et al., 2008). The magnetoelectroelastic fiber composites have been attracting extensive attention because of their enhanced magnetoelectric performance as well as the still open question in modeling. To achieve the 'tailored' properties (Zohdi, 2008), reasonable models for simulation of the macroscopic and microscopic response are necessary. Some classic micromechanical models for purely elastic problems are generalized to solve the magnetoelectroelastic problems in terms of an analogy between the governing equations of the magnetoelectroelastic problems and the purely elastic problems. These models include the dilute model (Zhang and Soh, 2005), self-consistent model (Nan, 1994; Srinivas and Li, 2005; Zhang and Soh, 2005), generalized self-consistent model

(Tong et al., 2008), Mori-Tanaka model (Dinzart and Sabar, 2011; Huang and Kuo, 1997; Li and Dunn, 1998; Srinivas et al., 2006; Wang and Pan, 2007; Wu and Huang, 2000; Zhang and Soh, 2005), composite cylinder assemblage model (Benveniste, 1995) and multi-inclusion model (Li, 2000). With these models some general analytical solutions for effective magnetoelectroelastic properties are presented by treating the inclusion interactions either approximately or in a statistically sense. As coupling moduli resulted from the interaction between the piezoelectric phase and the piezomagnetic phase, the magnetoelectric coefficients strongly depend on the inclusion interactions. From the existing researches, the magnetoelectric coefficient reaches the extremum usually at a relatively high inclusion volume fraction, where the inclusion interaction is strong. In consideration of these, high-order solutions of the magnetoelectric coefficient treating the inclusion interactions more accurately are necessary.

By adding another active interphase between the fiber and matrix of a two-phase composite, the three-phase magnetoelectroelastic fiber composites possess greater design flexibility. Several researches focus on such three-phase composites, such as multi-coated circular fibrous composites (Kuo and Pan, 2011), multi-coated elliptic fibrous composites (Kuo, 2011), composites with thinly coated inclusions (Dinzart and Sabar, 2011). Among these works, Kuo and Pan (2011) found that the magnetoelectric effect in coated composites can be enhanced by more than one order of magnitude as compared to the corresponding two-phase composite. However, an attendant problem of greater design flexibility is that more microscopic parameters influencing the effective properties need to be considered. Therefore, in order to optimize the numerous microscopic parameters to obtain extrema or desired magnitudes of effective magnetoelectroelastic properties, the solutions of the effective properties should cover all the key microscopic parameters.

In contrast to random microstructures, periodic microstructures usually exist in elaborately designed composites, since the design of an advanced composite is generally the one for a unit cell (Sun et al., 2001). Along with the progress of composites fabrication technology, some advanced magnetoelectroelastic composites with relatively rigorous periodic microstructures are invented. Recently, Zheng et al. (2004) reported a self-assembled multiferroic nanocomposite with hexagonal arrays of $CoFe_2O_4$ nanopillars embedded in a $BaTiO_3$ matrix. Boyd IV et al. (2003) presented a method for using arrays of micro-electro-mechanical systems electrodes and electromagnets to achieve microscale positioning of piezoelectric and piezomagnetic particles in liquid polymers. Shi et al. (2005) reported a kind of 1–3-type multiferroic and multifunctional composite with $Pb(Zr, Ti)O_3$ rod arrays embedded in a ferromagnetic medium of $(Tb, Dy)Fe_2$/epoxy produced by the dice-and-fill method. On the other hand, the periodic composite models provide useful limiting values of interacting inclusions from entirely disorder (random) to order (Nemat-Nasser and Hori, 1999). As far as the magnetoelectroelastic composites with a periodic array of fibers are concerned, Lee et al. (2005) performed a finite element analysis of a representative volume element to determine the effective magnetoelectroelastic moduli. Kuo and Pan (2011) generalized Rayleigh's formulism for the evaluation of the effective material properties in multicoated circular fibrous multiferroic composites. Camacho-Montes et al. (2009) and Espinosa-Almeyda et al. (2011) applied the asymptotic homogenization method to calculate the properties of the fiber composites and the ones with imperfect interfaces. Kuo (2011) combined the methods of complex potentials with a re-expansion formulae and the generalized Rayleigh's formulation to obtain a complete solution of the multi-field many-inclusion problem. The periodic microstructures considered in these researches are either hexagonal or square fiber arrays. Researches on the magnetoelectroelastic composites with a generally periodic array of fibers are not presented yet. Though, to the best of our knowledge, a real composite with such a periodic microstructure is not reported yet, such composites can be fabricated by the technique presented by Boyd IV et al. (2003). Furthermore, the magnetoelectroelastic composites with a generally periodic array of fibers are expected to exhibit a special magnetoelectric effect due to the overall anisotropy induced by general fiber arrays. That is, an electric field in one direction can result from a magnetic field in another perpendicular direction. Therefore, it is highly desirable to develop a method to analyze the magnetoelectric effect of such composites, especially the influence of the different fiber distributions and the anisotropy induced by general fiber arrays.

The present work is devoted to extend the eigenfunction expansion-variational method (EEVM) (Yan et al., 2011) to solve the anti-plane magnetoelectroelastic coupling problem for composites with a generally doubly periodic array of fibers. Series solutions in unified form for the effective magnetoelectroelastic moduli are presented, and then the validity and efficiency of such series solutions are verified. With the present solution, the influences of the volume fraction, permutation and the choice of the constituent phases, as well as the fiber distribution on the effective magnetoelectroelastic moduli are discussed. And then the influences of the volume fraction and interphase on interfacial stresses are discussed. Finally, the anisotropy of the composites induced by the general fiber arrays is discussed.

2. Statement and formulation of the problem

Consider a three-phase fiber composite subjected to combined anti-plane shear, inplane (Ox_1x_2-plane) electrical and magnetic loads as shown in Fig. 1, where the fiber, coating (interphase) and matrix are made of piezoelectric materials, piezomagnetic materials or inactive materials. The fibers are aligned in x_3 direction, the piezoelectric and piezomagnetic materials are polarized and magnetized along x_3-axis, respectively. Then only the anti-plane displacement w, inplane electrical potential ϕ and magnetic potential φ need to be considered, they are the functions of x_1 and x_2 only,

$$\{w, \phi, \varphi\} = \{w(x_1, x_2), \phi(x_1, x_2), \varphi(x_1, x_2)\} \tag{1}$$

For transversely isotropic piezoelectric materials and piezomagnetic materials, the anti-plane constitutive equations are

$$\begin{bmatrix} \tau_{i3} \\ D_i \end{bmatrix} = \begin{bmatrix} C_{44} & e_{15} \\ e_{15} & -\kappa_{11} \end{bmatrix} \begin{bmatrix} 2\varepsilon_{i3} \\ -E_i \end{bmatrix}, \begin{bmatrix} \tau_{i3} \\ B_i \end{bmatrix} = \begin{bmatrix} C_{44} & q_{15} \\ q_{15} & -\mu_{11} \end{bmatrix} \begin{bmatrix} 2\varepsilon_{i3} \\ -H_i \end{bmatrix}, \tag{2}$$

respectively. τ_{i3}, D_i and B_i ($i = 1, 2$) are the anti-plane shear stress and inplane electrical displacement and magnetic induction components, respectively; ε_{i3}, E_i and H_i ($i = 1, 2$) are the strain, electrical field and magnetic field components, respectively; C_{44}, e_{15}, q_{15}, κ_{11} and μ_{11} are the shear modulus, piezoelectric coefficient, piezomagnetic coefficient, dielectric permittivity and magnetic permittivity, respectively. The piezoelectric constitutive equation and piezomagnetic constitutive equation can be cast into the following unified form:

$$\begin{bmatrix} \tau_{i3} \\ D_i \\ B_i \end{bmatrix} = \begin{bmatrix} C_{44} & e_{15} & q_{15} \\ e_{15} & -\kappa_{11} & -a_{11} \\ q_{15} & -a_{11} & -\mu_{11} \end{bmatrix} \begin{bmatrix} 2\varepsilon_{i3} \\ -E_i \\ -H_i \end{bmatrix} \tag{3}$$

where a_{11} is the magnetoelectric coefficient, and is generally zero for monolithic piezoelectric materials and piezomagnetic materials.

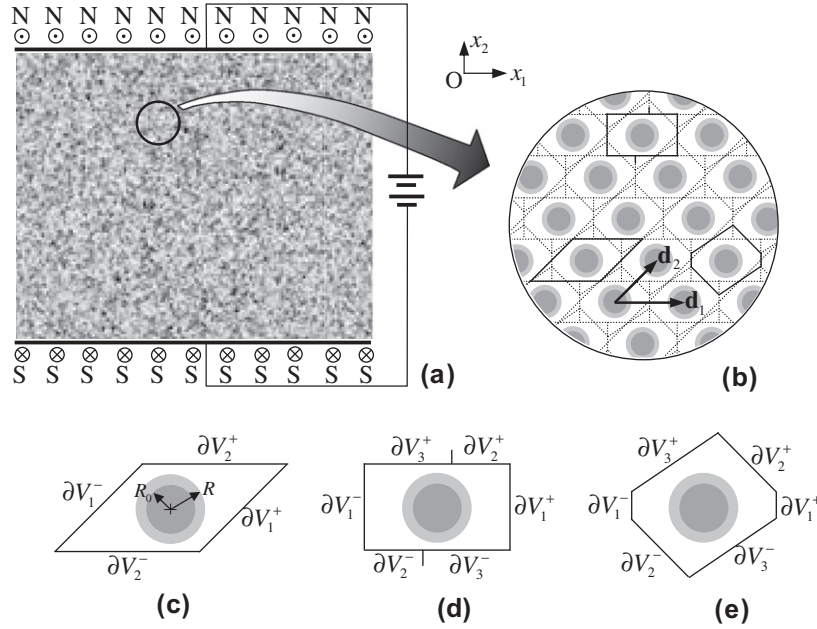For brevity and convenience, introduce the following matrix notations:

Fig. 1. Cross section of a three-phase magnetoelectroelastic fiber composite with a doubly periodic microstructure and its three types of unit cells. (a) Three-phase fiber composite subjected to combined anti-plane shear, inplane (Ox_1x_2 -plane) electrical and magnetic loads; (b) doubly periodic microstructure; (c) parallelogram unit cell; (d) staggered rectangular unit cell; (e) six-sided Voronoi unit cell.

$$\boldsymbol{w} = \begin{bmatrix} w \\ \phi \\ \varphi \end{bmatrix}, \quad \boldsymbol{\gamma}_1 = \begin{bmatrix} 2\varepsilon_{13} \\ -E_1 \\ -H_1 \end{bmatrix}, \quad \boldsymbol{\gamma}_2 = \begin{bmatrix} 2\varepsilon_{23} \\ -E_2 \\ -H_2 \end{bmatrix}, \quad \boldsymbol{\gamma} = \begin{bmatrix} 2\varepsilon_{13} & 2\varepsilon_{23} \\ -E_1 & -E_2 \\ -H_1 & -H_2 \end{bmatrix},$$

$$\boldsymbol{\tau}_1 = \begin{bmatrix} \tau_{13} \\ D_1 \\ B_1 \end{bmatrix}, \quad \boldsymbol{\tau}_2 = \begin{bmatrix} \tau_{23} \\ D_2 \\ B_2 \end{bmatrix}, \quad \boldsymbol{\tau} = \begin{bmatrix} \tau_{13} & \tau_{23} \\ D_1 & D_2 \\ B_1 & B_2 \end{bmatrix},$$

$$\boldsymbol{L} = \begin{bmatrix} C_{44} & e_{15} & q_{15} \\ e_{15} & -\kappa_{11} & -a_{11} \\ q_{15} & -a_{11} & -\mu_{11} \end{bmatrix}, \quad \nabla = \left[\frac{\partial}{\partial x_1}, \frac{\partial}{\partial x_2} \right], \quad \boldsymbol{x} = \begin{bmatrix} x_1 \\ x_2 \end{bmatrix}$$

$$(4)$$

where $\boldsymbol{w}$, $\boldsymbol{\gamma}$ and $\boldsymbol{\tau}$ are called the generalized displacement, strain and stress, respectively. In the absence of body forces, electric charge and electric current densities, the basic equations are put in matrix form:

gradient equation : $\quad \boldsymbol{\gamma} = \boldsymbol{w} \otimes \nabla$ (5a)

constitutive equation : $\quad \boldsymbol{\tau} = \boldsymbol{L}\boldsymbol{\gamma}$ (5b)

equilibrium equation : $\quad \nabla \boldsymbol{\tau}^T = 0$ (5c)

where the superscript "T" denotes transpose.

From Eqs. (5a), (5b), (5c), the generalized displacement satisfies the following Laplace's equation:

$$\nabla^2 \boldsymbol{w} = 0 \tag{6}$$

where $\nabla^2 \left(= \frac{\partial^2}{\partial x_1^2} + \frac{\partial^2}{\partial x_2^2} \right)$ is the Laplacian operator. Therefore, the generalized displacement $\boldsymbol{w}$ can be formulated by three potentials $\{f_1(z), f_2(z), f_3(z)\}$ with a vector form $\boldsymbol{f}(z)$, and from Eqs. (5a), (5b), (5c), the generalized stress $\boldsymbol{\tau}$ and the resultant force $\boldsymbol{T}$ can be formulated as:

$$\boldsymbol{w} = \frac{1}{2} [\boldsymbol{f}(z) + \overline{\boldsymbol{f}(z)}] \tag{7a}$$

$$\boldsymbol{\tau}_1 - i\boldsymbol{\tau}_2 = \boldsymbol{L}\boldsymbol{f}'(z) \tag{7b}$$

$$\boldsymbol{T} = \int_A^B \boldsymbol{\tau} \boldsymbol{n} dS = \frac{1}{2i} \boldsymbol{L} [\boldsymbol{f}(z) - \overline{\boldsymbol{f}(z)}]_A^B \tag{7c}$$

where, $z = x_1 + ix_2$ is a complex variable, the over bar denotes the complex conjugate, the prime denotes the derivative with respect to z, $[\cdot]_A^B$ denotes the difference of the values of the bracketed function from point A to point B.

3. Eigenfunction expansion-variational method

Now extend the eigenfunction expansion-variational method (EEVM) (Yan et al., 2011) to cover the anti-plane magnetoelectroelastic coupling problem for composites with a generally doubly periodic fiber array.

3.1. Eigenfunction expansion of the complex potentials

As shown in Fig. 1((c)–(e)), a typical unit cell of a three-phase fiber composite is divided into three regions occupied, respectively, by a fiber, a coating (interphase) and a surrounding matrix. Subscripts/Superscripts "*f*", "*c*" and "*m*" refer to the fiber, coating and matrix, respectively. R_0 and R are the radius of the fiber and the external radius of the coating, respectively.

The complex potential $\boldsymbol{f}_f(z)$ in the fiber region can be expanded into a Taylor series, $\boldsymbol{f}_c(z)$ in the coating region and $\boldsymbol{f}_m(z)$ in the matrix region can be expanded into Laurent series,

$$\boldsymbol{f}_f(\boldsymbol{Z}) = \sum_{n=1}^{\infty} \boldsymbol{C}_n^{(1)} \boldsymbol{Z}^{2n-1} \tag{8a}$$

$$\boldsymbol{f}_c(\boldsymbol{Z}) = \sum_{n=1}^{\infty} \boldsymbol{C}_n^{(2)} \boldsymbol{Z}^{-(2n-1)} + \sum_{n=1}^{\infty} \boldsymbol{C}_n^{(3)} \boldsymbol{Z}^{2n-1} \tag{8b}$$

$$\boldsymbol{f}_m(\boldsymbol{Z}) = \sum_{n=1}^{\infty} \boldsymbol{C}_n^{(4)} \boldsymbol{Z}^{-(2n-1)} + \sum_{n=1}^{\infty} \boldsymbol{C}_n^{(5)} \boldsymbol{Z}^{2n-1} \tag{8c}$$

where $\boldsymbol{C}_n^{(1)}, \boldsymbol{C}_n^{(2)}, \boldsymbol{C}_n^{(3)}, \boldsymbol{C}_n^{(4)}$ and $\boldsymbol{C}_n^{(5)}$ are complex coefficient vectors. Due to the centrosymmetry of the unit cell, only the odd terms in Eqs. (8a), (8b), (8c) remain.

The continuity conditions of the generalized resultant force $\boldsymbol{T}$ and the generalized displacement $\boldsymbol{w}$ across the fiber-coating and coating-matrix interfaces:

$$\boldsymbol{T}_{\rm f} = \boldsymbol{T}_{\rm c}, \quad \boldsymbol{w}_{\rm f} = \boldsymbol{w}_{\rm c} \quad \text{at } |z| = R_0 \tag{9a}$$

$$\boldsymbol{T}_{\rm c} = \boldsymbol{T}_{\rm m}, \quad \boldsymbol{w}_{\rm c} = \boldsymbol{w}_{\rm m} \quad \text{at } |z| = R \tag{9b}$$

can provide four sets of equations with respect to five sets of unknown complex coefficients $\boldsymbol{C}_n^{(1)}, \boldsymbol{C}_n^{(2)}, \boldsymbol{C}_n^{(3)}, \boldsymbol{C}_n^{(4)}$ and $\boldsymbol{C}_n^{(5)}$:

$$\begin{cases} \boldsymbol{C}_n^{(1)} = \boldsymbol{C}_n^{(3)} + \bar{\boldsymbol{C}}_n^{(2)} R_0^{-2(2n-1)} \\ \boldsymbol{L}_{\rm f}\boldsymbol{C}_n^{(1)} = \boldsymbol{L}_{\rm c}(\boldsymbol{C}_n^{(3)} - \bar{\boldsymbol{C}}_n^{(2)} R_0^{-2(2n-1)}) \\ \boldsymbol{C}_n^{(3)} + \bar{\boldsymbol{C}}_n^{(2)} R^{-2(2n-1)} = \boldsymbol{C}_n^{(5)} + \bar{\boldsymbol{C}}_n^{(4)} R^{-2(2n-1)} \\ \boldsymbol{L}_{\rm c}(\boldsymbol{C}_n^{(3)} - \bar{\boldsymbol{C}}_n^{(2)} R^{-2(2n-1)}) = \boldsymbol{L}_{\rm m}(\boldsymbol{C}_n^{(5)} - \bar{\boldsymbol{C}}_n^{(4)} R^{-2(2n-1)}) \end{cases} \tag{10}$$

Only one set of independent unknown complex coefficients (choose $\boldsymbol{C}_n^{(5)}$) remains. By solving Eq. (10), one obtains the relation between $\boldsymbol{C}_n^{(4)}$ and $\boldsymbol{C}_n^{(5)}$:

$$\boldsymbol{C}_n^{(4)} = \boldsymbol{\eta}_n R^{4n-2} \bar{\boldsymbol{C}}_n^{(5)} \tag{11}$$

where

$$\boldsymbol{\eta}_n = \left[\boldsymbol{I} + (\boldsymbol{I} + \boldsymbol{L}_{\rm c}^{-1}\boldsymbol{L}_{\rm m})^{-1} \boldsymbol{\eta}_{\rm fc}(\boldsymbol{L}_{\rm c}^{-1}\boldsymbol{L}_{\rm m} - \boldsymbol{I})\xi^{2n-1} \right]^{-1} [(\boldsymbol{I} + \boldsymbol{L}_{\rm c}^{-1}\boldsymbol{L}_{\rm m})^{-1} \boldsymbol{\eta}_{\rm fc}(\boldsymbol{I} + \boldsymbol{L}_{\rm c}^{-1}\boldsymbol{L}_{\rm m})\xi^{2n-1} + \boldsymbol{\eta}_{\rm cm}] \tag{12}$$

$$\xi = R_0^2 / R^2 \tag{13}$$

$$\boldsymbol{\eta}_{\rm fc} = (\boldsymbol{L}_{\rm f} + \boldsymbol{L}_{\rm c})^{-1}(\boldsymbol{L}_{\rm c} - \boldsymbol{L}_{\rm f}) \tag{14}$$

$$\boldsymbol{\eta}_{\rm cm} = (\boldsymbol{L}_{\rm c} + \boldsymbol{L}_{\rm m})^{-1}(\boldsymbol{L}_{\rm m} - \boldsymbol{L}_{\rm c}) \tag{15}$$

and $\boldsymbol{I}$ is the 3×3 identity matrix. From Eqs. (8c) and (11), the eigenfunction expansion of the complex potential $\boldsymbol{f}_{\rm m}(z)$ can be written as:

$$\boldsymbol{f}_{\rm m}(\boldsymbol{z}) = \sum_{n=1}^{\infty} \boldsymbol{\eta}_n R^{4n-2} \bar{\boldsymbol{C}}_n^{(5)} \boldsymbol{z}^{-(2n-1)} + \boldsymbol{C}_n^{(5)} \boldsymbol{z}^{2n-1} \tag{16}$$

It is worth noting that the parameter matrix $\boldsymbol{\eta}_n$ in Eq. (16) contains all the parameters of the constituent properties and the relative volume fraction of the interphase.

The remaining work is to determine one set of unknown coefficients, $\boldsymbol{C}_n^{(5)}$, which can be completed by using the periodic boundary conditions of the unit cell.

3.2. Periodicity conditions and variational functional for a unit cell

Consider the three-phase fiber composite with a doubly periodic microstructure as shown in Fig. 1(b). $\boldsymbol{d}_1$ and $\boldsymbol{d}_2$ denote two fundamental periods. For the magnetoelectroelastic behavior considered here, the generalized displacement is doubly quasiperiodic and the generalized stress is doubly periodic.

Due to the periodicity of the microstructure and the magnetoelectroelastic field, unit cells are picked out for analysis. Three kinds of typical unit cells: parallelogram unit cell, staggered rectangular unit cell, six-sided Voronoi unit cell, are selected as shown in Fig. 1(c)–(e). The parallelogram unit cell has two couples of opposite edges along the two fundamental periods respectively, hence indicates the double periodicity directly; the staggered rectangular unit cell has two geometric parameters (the side length ratio and relative staggered distance) which can directly show the variation of the doubly periodic microstructure, and will be used later; the six-sided Voronoi unit cell can cover the largest fiber volume fraction, hence can be used to analyze the extreme cases of fibers nearly touching each other. The boundaries of each unit cell can be divided into $\partial V^+ = \sum_s \partial V_s^+$ and $\partial V^- = \sum_s \partial V_s^-$, where $s = 1$,

2 in Fig. 1(c) and $s = 1, 2, 3$ in Fig. 1(d) and (e). By a proper translation $\boldsymbol{p}^s$, the boundary ∂V_s^- will coincide with the boundary ∂V_s^+, where $\boldsymbol{p}^1 = \boldsymbol{d}_1$ and $\boldsymbol{p}^2 = \boldsymbol{d}_2$ in Fig. 1(c) and $\boldsymbol{p}^1 = \boldsymbol{d}_1$, $\boldsymbol{p}^2 = \boldsymbol{d}_2$ and $\boldsymbol{p}^3 = \boldsymbol{d}_2 - \boldsymbol{d}_1$ in Fig. 1(d) and (e). The periodic boundary conditions of a unit cell can be written as:

$$\begin{cases} \boldsymbol{w}^{s+} - \boldsymbol{w}^{s-} = \langle\boldsymbol{\gamma}\rangle\boldsymbol{p}^s \\ \boldsymbol{t}^{s+} + \boldsymbol{t}^{s-} = 0 \end{cases} \tag{17}$$

where $\langle\boldsymbol{\gamma}\rangle$ denotes the average of the generalized strain $\boldsymbol{\gamma}$ over a unit cell; $\boldsymbol{t}(=\tau\boldsymbol{n})$ denotes the generalized boundary stress consisting of the boundary stress, electrical displacement and magnetic induction; $\boldsymbol{n}$ denotes the unit normal vector on the boundary; the quantities with superscripts "$s-$" and "$s+$" are corresponding to taking values from ∂V_s^- and ∂V_s^+, respectively.

By using the Lagrangian multiplier method, the periodic boundary conditions (17) of a unit cell can be incorporated into the functional for the magnetoelectroelastic issue under consideration. The stationary condition of the function (Yan et al., 2011) is:

$$\sum_s \int_{\partial V_s^+} \delta\boldsymbol{t}^{s+} \cdot (\boldsymbol{w}^{s+} - \boldsymbol{w}^{s-})dS - \sum_s \int_{\partial V_s^+} (\boldsymbol{t}^{s+} + \boldsymbol{t}^{s-}) \cdot \delta\boldsymbol{w}^{s-}dS$$
$$= \sum_s \int_{\partial V_s^+} \delta\boldsymbol{t}^{s+} \cdot \langle\boldsymbol{\gamma}\rangle\boldsymbol{p}^s dS \tag{18}$$

This stationary condition is applicable to unit cells in any shape, and from any periodic microstructure, whatever the symmetry.

3.3. Determination of the unknown coefficients

Substituting Eq. (16) into Eqs. (7a), (7b), (7c), and taking an appropriate truncation, the expansions of the generalized stresses, displacement, boundary stress and resultant force can be written as:

$$\boldsymbol{\tau}_i = \sum_{n=1}^{2N} \boldsymbol{L}_{\rm m}\boldsymbol{\tau}_i^{(n)}\boldsymbol{X}_n, \quad \boldsymbol{w} = \sum_{n=1}^{2N} \boldsymbol{w}^{(n)}\boldsymbol{X}_n, \quad \boldsymbol{t} = \sum_{n=1}^{2N} \boldsymbol{L}_{\rm m}\boldsymbol{t}^{(n)}\boldsymbol{X}_n,$$
$$\boldsymbol{T} = \sum_{n=1}^{2N} \boldsymbol{L}_{\rm m}\boldsymbol{T}^{(n)}\boldsymbol{X}_n \quad i = 1,2 \tag{19}$$

where

$$\boldsymbol{X}_n = \begin{cases} \boldsymbol{C}_n^{(5)} & 1 \le n \le N \\ \bar{\boldsymbol{C}}_{n-N}^{(5)} & N+1 \le n \le 2N \end{cases} \tag{20a}$$

$$\boldsymbol{\tau}_1^{(n)} = \begin{cases} \frac{1}{2}[\boldsymbol{I}(2n-1)z^{2n-2} + \boldsymbol{\eta}_n R^{4n-2}(1-2n)\bar{z}^{-2n}] & 1 \le n \le N \\ \frac{1}{2}[\boldsymbol{I}(2n-2N-1)\bar{z}^{2n-2N-2} + \boldsymbol{\eta}_{n-N} R^{4n-4N-2}(1-2n+2N)z^{-2n+2N}] & N+1 \le n \le 2N \end{cases} \tag{20b}$$

$$\boldsymbol{\tau}_2^{(n)} = \begin{cases} -\frac{1}{2i}[\boldsymbol{I}(2n-1)z^{2n-2} - \boldsymbol{\eta}_n R^{4n-2}(1-2n)\bar{z}^{-2n}] & 1 \le n \le N \\ -\frac{1}{2i}[-\boldsymbol{I}(2n-2N-1)\bar{z}^{2n-2N-2} + \boldsymbol{\eta}_{n-N} R^{4n-4N-2}(1-2n+2N)z^{-2n+2N}] & N+1 \le n \le 2N \end{cases} \tag{20c}$$

$$\boldsymbol{w}^{(n)} = \begin{cases} \frac{1}{2}[\boldsymbol{I}z^{2n-1} + \boldsymbol{\eta}_n R^{4n-2}\bar{z}^{1-2n}] & 1 \le n \le N \\ \frac{1}{2}[\boldsymbol{I}\bar{z}^{2n-2N-1} + \boldsymbol{\eta}_{n-N} R^{4n-4N-2}z^{1-2n+2N}] & N+1 \le n \le 2N \end{cases} \tag{20d}$$

$$\boldsymbol{t}^{(n)} = \boldsymbol{\tau}^{(n)}\boldsymbol{n} \quad 1 \le n \le 2N \tag{20e}$$

$$\boldsymbol{T}^{(n)} = \begin{cases} \frac{1}{2i}[\boldsymbol{I}z^{2n-1} - \boldsymbol{\eta}_n R^{4n-2}\bar{z}^{1-2n}]_{\rm A}^{\rm B} & 1 \le n \le N \\ \frac{1}{2i}[-\boldsymbol{I}\bar{z}^{2n-2N-1} + \boldsymbol{\eta}_{n-N} R^{4n-4N-2}z^{1-2n+2N}]_{\rm A}^{\rm B} & N+1 \le n \le 2N \end{cases} \tag{20f}$$

If the unit cell shapes and boundary conditions are simultaneously axisymmetric, the expansions (Eqs. (20a)–(20f)) can be reduced as

listed in (Yan et al., 2011). The substitution of Eq. (19) into the stationary condition (18) yields the following linear algebraic equations:

$$\sum_{m=1}^{2N} \boldsymbol{A}_{nm}\boldsymbol{X}_m = \boldsymbol{B}_n \quad n = 1, 2, \ldots, 2N \tag{21a}$$

where

$$\boldsymbol{A}_{nm} = \sum_s \int_{\partial V_s^+} (\boldsymbol{t}_{(n)}^{s+})^T \boldsymbol{L}_m (\boldsymbol{w}_{(m)}^{s+} - \boldsymbol{w}_{(m)}^{s-}) dS$$

$$- \sum_s \int_{\partial V_s^+} (\boldsymbol{w}_{(n)}^{s-})^T \boldsymbol{L}_m (\boldsymbol{t}_{(m)}^{s+} + \boldsymbol{t}_{(m)}^{s-}) dS \tag{21b}$$

$$\boldsymbol{B}_n = \sum_s \int_{\partial V_s^+} (\boldsymbol{t}_{(n)}^{s+})^T \boldsymbol{L}_m (\langle\boldsymbol{\gamma}\rangle \boldsymbol{p}^s) dS = \sum_s (\boldsymbol{T}_{(n)}^{s+})^T \boldsymbol{L}_m (\langle\boldsymbol{\gamma}\rangle \boldsymbol{p}^s) \tag{21c}$$

$\boldsymbol{t}_{(n)}^{s+}$, $\boldsymbol{w}_{(m)}^{s+}$ and $\boldsymbol{T}_{(n)}^{s+}$ denote taking the values of $\boldsymbol{t}^{(n)}$, $\boldsymbol{w}^{(m)}$ and $\boldsymbol{T}^{(n)}$ from ∂V_s^+, respectively; and the quantities with the superscript "$s-$" are corresponding to taking values from ∂V_s^-. As all the parameters of the constituent properties and the relative volume fraction of the interphase are packed into the parameter matrix $\boldsymbol{\eta}_n$, the present solutions are in unified form for various of two-phase and three phase magnetoelectroelastic fiber composites.

4. Effective magnetoelectroelastic moduli

The effective magnetoelectroelastic moduli of a composite, $\boldsymbol{L}_{ij}^e$, are calculated on the average fields over a unit cell (Nemat-Nasser and Hori, 1999), that is

$$\langle\boldsymbol{\tau}_i\rangle = \boldsymbol{L}_{ij}^e \langle\boldsymbol{\gamma}_j\rangle \quad i, j = 1, 2 \tag{22}$$

where $\langle\boldsymbol{\tau}_i\rangle$ is the average generalized stress, which can be calculated by the following formula:

$$\langle\boldsymbol{\tau}_i\rangle = \frac{1}{V} \int_V \boldsymbol{\tau}_i dV = \frac{1}{V} \sum_s \boldsymbol{T}^{s+} p_i^s \tag{23}$$

$\boldsymbol{T}^{s+}$ is the generalized resultant force on the boundary ∂V_s^+, V is the volume of the unit cell. The implementing procedure is that the periodic boundary conditions (17) with a given average generalized strain $\langle\boldsymbol{\gamma}_j\rangle$ are prescribed for the unit cell, and then the average generalized stress $\langle\boldsymbol{\tau}_i\rangle$ is solved for calculating the effective moduli. From Eqs. (19), (21a), (21b), (21c), and (23) the average generalized stress can be calculated by

$$\langle\boldsymbol{\tau}_i\rangle = \boldsymbol{L}_m \frac{1}{V} \sum_{n=1}^{2N}\sum_{m=1}^{2N} \left(\sum_s \boldsymbol{T}_{(n)}^{s+} p_i^s\right)(\boldsymbol{A}^{-1})_{nm}\left(\sum_s \boldsymbol{T}_{(m)}^{s+} p_j^s\right)\langle\boldsymbol{\gamma}_j\rangle \tag{24}$$

By comparing Eq. (22) and Eq. (24), one obtains

$$\boldsymbol{L}_{ij}^e = \boldsymbol{L}_m \frac{1}{V} \sum_{n=1}^{2N}\sum_{m=1}^{2N} \left(\sum_s \boldsymbol{T}_{(n)}^{s+} p_i^s\right)(\boldsymbol{A}^{-1})_{nm}\left(\sum_s \boldsymbol{T}_{(m)}^{s+} p_j^s\right) \tag{25}$$

which is in unified from for composites with different fiber arrays. When the term number N of the eigenfunction expansion is large enough, the series solutions of the effective moduli will approach the exact ones.

For a composite with a generally periodic array of fibers, the overall magnetoelectroelastic behavior in two directions may be coupled, and a general form of the effective moduli is

$$\boldsymbol{L}_{11}^e = \begin{bmatrix} C_{55}^e & e_{15}^e & q_{15}^e \\ e_{15}^e & -\kappa_{11}^e & -a_{11}^e \\ q_{15}^e & -a_{11}^e & -\mu_{11}^e \end{bmatrix}, \quad \boldsymbol{L}_{22}^e = \begin{bmatrix} C_{44}^e & e_{24}^e & q_{24}^e \\ e_{24}^e & -\kappa_{22}^e & -a_{22}^e \\ q_{24}^e & -a_{22}^e & -\mu_{22}^e \end{bmatrix}, \quad \boldsymbol{L}_{21}^e = \begin{bmatrix} C_{45}^e & e_{14}^e & q_{14}^e \\ e_{25}^e & -\kappa_{21}^e & -a_{21}^e \\ q_{25}^e & -a_{12}^e & -\mu_{21}^e \end{bmatrix},$$

$$\boldsymbol{L}_{12}^e = \begin{bmatrix} C_{54}^e & e_{25}^e & q_{25}^e \\ e_{14}^e & -\kappa_{12}^e & -a_{12}^e \\ q_{14}^e & -a_{21}^e & -\mu_{12}^e \end{bmatrix} \tag{26}$$

For a composite with a square or hexagonal array of fibers, according to the symmetry, the overall magnetoelectroelastic behavior exhibits transverse isotropy, that is

$$\boldsymbol{L}_{11}^e = \boldsymbol{L}_{22}^e, \quad \boldsymbol{L}_{12}^e = \boldsymbol{L}_{21}^e = 0 \tag{27}$$

Let $\boldsymbol{L}_e = \boldsymbol{L}_{11}^e = \boldsymbol{L}_{22}^e$ for a transversely isotropic composite.

5. Numerical examples and discussions

We have obtained a unified series solution by using the eigenfunction expansion-variational method (EEVM) for the effective magnetoelectroelastic moduli of three-phase fiber composites with doubly periodic microstructures. First, the validity and efficiency of the present solution are verified. Second, by using the present solution, the influences of the volume fraction, permutation and the choice of the constituent phases on the effective magnetoelectric moduli are investigated. Finally, the influence of the fiber distribution and the distribution-induced anisotropy of the effective magnetoelectric moduli are discussed.

Three typical materials composing the magnetoelectroelastic composites are cited in the calculation, whose properties are listed in Table 1.

5.1. Validity and efficiency

To verify the validity and efficiency of the present series solution, convergence analysis is conducted. Consider three fiber arrays, i.e., square array ($\boldsymbol{d}_1 = |\boldsymbol{d}_1|\{1, 0\}$, $\boldsymbol{d}_2 = |\boldsymbol{d}_1|\{0, 1\}$), hexagonal array ($\boldsymbol{d}_1 = |\boldsymbol{d}_1|\{1, 0\}$, $\boldsymbol{d}_2 = |\boldsymbol{d}_1|\{\cos 60°, \sin 60°\}$), and a generally doubly periodic array ($\boldsymbol{d}_1 = |\boldsymbol{d}_1|\{1, 0\}$, $\boldsymbol{d}_2 = 1.2|\boldsymbol{d}_1|\{\cos 75°, \sin 75°\}$); and a relatively high volume fraction $\lambda = 0.6$ (λ is the fiber volume fraction for a two-phase composite and is the total fraction of the fiber and interphase for a three-phase composite). The variations of the effective magnetoelectroelastic moduli with the term number N of the eigenfunction expansion are listed in Tables 2–5. A rapid convergence of the present solution is observed.

In Tables 2 and 3, a two-phase composite (fiber/matrix = $BaTiO_3/CoFe_2O_4$) and a three-phase composite (fiber/interphase/matrix = $BaTiO_3$/Terfenol-D/$CoFe_2O_4$, $R_0/R = 4/5$) with a square fiber array are considered, respectively. The results of the effective magnetoelectroelastic moduli ($C_{44}^e, e_{15}^e, \kappa_{11}^e, q_{15}^e, \mu_{11}^e, a_{11}^e$) are in good agreement with those predicted by Kuo (2011). In Table 4, a three-phase composite ($BaTiO_3$/Terfenol-D/$CoFe_2O_4$, $R_0/R = 4/5$) with a hexagonal fiber array is considered, and it is observed that the results converge more rapidly than those for a square fiber array. To the best of our knowledge, neither analytical nor numerical results of effective magnetoelectroelastic moduli of three-phase composites with a hexagonal fiber array were reported.

In Table 5, a three-phase composite ($BaTiO_3$/Terfenol-D/$CoFe_2O_4$, $R_0/R = 4/5$) with a generally doubly periodic fiber array is considered. In such a general case, there exist two coupling magnetoelectric coefficients (a_{12}^e and a_{21}^e) besides two main magnetoelectric coefficients (a_{11}^e and a_{22}^e), which shows the composite is anisotropic. Since for the same general fiber array, three kinds of typical unit cells: parallelogram unit cell, staggered rectangular unit cell and six-sided

Table 1
Magnetoelectroelastic materials properties.

	BaTiO$_3$	CoFe$_2$O$_4$	Terfenol-D
C_{44} (GPa)	43	45.3	13.6
e_{15} (C/m^2)	11.6	0	0
κ_{11} (nF/m)	11.2	0.08	0.05
q_{15} (N/Am)	0	550	108.3
μ_{11} (10^{-6} N/A^2)	5	590	5.4
a_{11} (10^{-12} Ns/VC)	0	0	0

Table 2
Variation of the effective magnetoelectroelastic moduli with the term number N of the eigenfunction expansion and a comparison with those predicted by Kuo (2011), for a two-phase composite (BaTiO$_3$/CoFe$_2$O$_4$) with the square fiber array ($\boldsymbol{d}_1 = |\boldsymbol{d}_1|\{1,0\}$, $\boldsymbol{d}_2 = |\boldsymbol{d}_1|\{0,1\}$) and BaTiO$_3$ volume fraction $\lambda = 0.6$.

N	BaTiO$_3$/CoFe$_2$O$_4$ (Square array)					
	C_{44}^e (GPa)	e_{15}^e (C/m^2)	κ_{11}^e (nF/m)	q_{15}^e (N/Am)	μ_{11}^e (10^{-6} Ns^2/C^2)	$-a_{11}^e$ (10^{-12} Ns/VC)
1	50.78	0.2768	0.3544	163.4	178.7	5.562
3	50.79	0.2596	0.3379	130.7	143.8	5.987
5	50.79	0.2587	0.3370	128.1	141.1	6.019
7	50.79	0.2588	0.3371	128.0	141.0	6.020
9	50.79	0.2588	0.3371	128.0	141.0	6.020
Kuo	50.8	0.255	0.337	128	140	6.03

Table 3
Variation of the effective magnetoelectroelastic moduli with the term number N of the eigenfunction expansion and a comparison with those predicted by Kuo (2011), for a three-phase composite (BaTiO$_3$/Terfenol-D/CoFe$_2$O$_4$) with the square fiber array ($\boldsymbol{d}_1 = |\boldsymbol{d}_1|\{1,0\}$, $\boldsymbol{d}_2 = |\boldsymbol{d}_1|\{0,1\}$), a total volume fraction of BaTiO$_3$ and Terfenol-D $\lambda = 0.6$, and a relative radius of BaTiO$_3$ fiber $R_0/R = 4/5$.

N	BaTiO$_3$/Terfenol-D/CoFe$_2$O$_4$ (Square array)					
	C_{44}^e (GPa)	e_{15}^e (C/m^2)	κ_{11}^e (nF/m)	q_{15}^e (N/Am)	μ_{11}^e (10^{-6} Ns^2/C^2)	$-a_{11}^e$ (10^{-12} Ns/VC)
1	37.14	0.06011	0.1466	206.1	178.8	67.59
3	37.05	0.05821	0.1438	178.4	144.0	61.28
5	37.04	0.05807	0.1436	176.3	141.4	60.63
7	37.04	0.05807	0.1436	176.2	141.3	60.59
9	37.04	0.05807	0.1436	176.2	141.2	60.59
Kuo	37.0	0.0599	0.147	175	140	63.0

Table 4
Variation of the effective magnetoelectroelastic moduli with the term number N of the eigenfunction expansion for a three-phase composite (BaTiO$_3$/Terfenol-D/CoFe$_2$O$_4$) with the hexagonal fiber array ($\boldsymbol{d}_1 = |\boldsymbol{d}_1|\{1,0\}$, $\boldsymbol{d}_2 = |\boldsymbol{d}_1|\{\cos 60°, \sin 60°\}$), a total volume fraction of BaTiO$_3$ and Terfenol-D $\lambda = 0.6$, and a relative radius of BaTiO$_3$ fiber $R_0/R = 4/5$.

| N	BaTiO$_3$/Terfenol-D /CoFe$_2$O$_4$ (Hexagonal array)					
	C_{44}^e (GPa)	e_{15}^e (C/m$_2$)	κ_{11}^e (nF/m)	q_{15}^e (N/Am)	μ_{11}^e (10^{-6} Ns^2/C^2)	$-a_{11}^e$ (10^{-12} Ns/VC)
1	37.07	0.05838	0.1441	191.2	160.4	64.67
3	37.05	0.05794	0.1430	184.0	151.4	63.44
5	37.05	0.05794	0.1430	184.1	151.4	63.46
7	37.05	0.05794	0.1435	184.0	151.4	63.45
9	37.05	0.05794	0.1435	184.0	151.4	63.45

Voronoi unit cell (Fig. 1(c)–(e)), can be picked out for calculation, the corresponding results can be compared and verified with each other. With the increasing of the term number N, a perfect agreement is reached, which demonstrates a good self-consistency of the present unified solution.

5.2. Influences of the volume fraction, permutation and choice of the phases

The prime concern about magnetoelectroelastic composites is to obtain the maximum magnitude of the effective magnetoelectric coefficients, which can be reached by optimizing the volume fraction, permutation and choice of the constituent phases. There are one piezoelectric phase (BaTiO$_3$) and two piezomagnetic phases (CoFe$_2$O$_4$ and Terfenol-D) in Table 1 to choose from. For cylindrical fiber composites shown in Fig. 1, it should be noted that the largest allowable fiber volume fraction is 0.785 for a square fiber array, and 0.906 for a hexagonal fiber array, and 1 for an idealized even fiber distribution in the Mori-Tanaka estimation (Wang and Pan, 2007).

Table 5
Variation of the effective magnetoelectroelastic moduli with the term number N of the eigenfunction expansion for a three-phase composite (BaTiO$_3$/Terfenol-D/CoFe$_2$O$_4$) with a generally doubly periodic fiber array ($\boldsymbol{d}_1 = |\boldsymbol{d}_1|\{1,0\}$, $\boldsymbol{d}_2 = 1.2|\boldsymbol{d}_1|\{\cos 75°, \sin 75°\}$), a total volume fraction of BaTiO$_3$ and Terfenol-D $\lambda = 0.6$, and a relative radius of BaTiO$_3$ fiber $R_0/R = 4/5$.

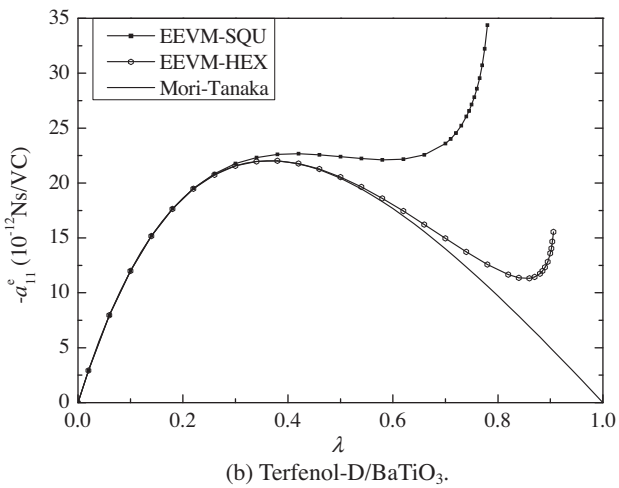| N	Magnetoelectric coefficients: 10^{-12} Ns/VC (BaTiO$_3$/Terfenol-D/CoFe$_2$O$_4$)								
	Parallelogram unit cell			Staggered rectangular unit cell			Voronoi unit cell		
	$-a_{11}^e$	$-a_{22}^e$	$-a_{12}^e$	$-a_{11}^e$	$-a_{22}^e$	$-a_{12}^e$	$-a_{11}^e$	$-a_{22}^e$	$-a_{12}^e$
1	70.82	63.98	−1.996	68.62	63.40	0.2642	69.53	61.73	0.6479
3	68.74	55.63	0.2091	68.76	55.00	0.6091	68.68	54.54	0.4027
5	68.60	53.70	0.1971	68.60	53.54	0.1579	68.62	53.39	0.1251
7	68.60	53.32	0.1793	68.62	78.53	0.9441	68.60	53.22	0.1506
9	68.60	53.30	0.1780	68.60	53.19	0.1524	68.60	53.20	0.1536
11	68.60	53.17	0.1511	68.60	53.18	0.1521	68.60	53.18	0.1520
13	68.60	53.18	0.1520	68.60	53.18	0.1520	68.60	53.18	0.1520

5.2.1. Two-phase composites

The effective magnetoelectric coefficient ($a_{11}^e = a_{22}^e$) versus the fiber volume fraction is depicted in Fig. 2(a) and b for the two-phase composites: BaTiO$_3$/CoFe$_2$O$_4$ and Terfenol-D/BaTiO$_3$, respectively. The present series solutions for a square fiber array and a hexagonal fiber array are compared with the Mori-Tanaka estimation as well. From Fig. 2(a) for composite BaTiO$_3$/CoFe$_2$O$_4$, it is seen that $|a_{11}^e|$ reaches the maximum at a high fiber volume fraction ($\lambda = 0.76$ for the square array, 0.84 for the hexagonal array and 0.86 for the Mori-Tanaka estimation), and then decreases rapidly with the BaTiO$_3$ fiber volume fraction increasing before the fibers contact together. In this case the stationary value of $|a_{11}^e|$ is also the absolute maximum as usually depicted. The Mori-Tanaka estimation is closer to results for the hexagonal fiber array. From Fig. 2(b) for composite Terfenol-D/BaTiO$_3$, it is seen that, with the Terfenol-D fiber volume fraction increasing, the $|a_{11}^e|$ first increases and reaches a local maximum (stationary value), then decreases slightly, finally increases rapidly till fibers contact together. In this case, there is another local maximum of $|a_{11}^e|$ at the end point (fibers contact) besides the stationary value, and the stationary value is not the absolute maximum for the square fiber array. It is seen that for a small fiber volume fraction, the results by the present method are in agreement with those by the Mori-Tanaka method. However, for a large fiber volume fraction, interactions between fibers are strong and then the influence of the fiber distribution is significant, the Mori-Tanaka method fails to predict the correct results and the present method is required.

The Mori-Tanaka method accounts for the interaction of fibers only in a statistical sense, thus the fiber volume fraction can approach 1. In fact, the maximum allowable fiber volume fractions are 0.785 for a square array of cylindrical fibers and 0.906 for a hexagonal array, respectively. At the maximum allowable fiber volume fraction, the matrix still exists, thus the effective magnetoelectric coefficient is usually not zero. Moreover, when fibers contact together at the maximum fiber volume fraction, the matrix is separated by the fibers, the continuous phase and the dispersive phase are reversed. Near such a reversal point, a sudden change of the magnetoelectric coefficient may happen. For a hexagonal fiber array, the volume fraction of matrix is very low (0.094, less than 0.1) when fibers contact, thus such a sudden change is weak. In Fig. 2(b), the $|a_{11}^e|$ of the composite Terfenol-D/BaTiO$_3$ increases sharply when fibers almost contact together. From this phenomenon it can be reasoned that the $|a_{11}^e|$ of the composite BaTiO$_3$/Terfenol-D may be much larger than that of the composite Terfenol-D/BaTiO$_3$, which will be verified in Fig. 3.

Motivated by the different phenomena revealed in Fig. 2(a) and (b), in order to investigate the influence of the permutation and choice of the phases, a comparison of four kinds of two-phase composites is depicted in Fig. 3 for a hexagonal fiber array. It is seen
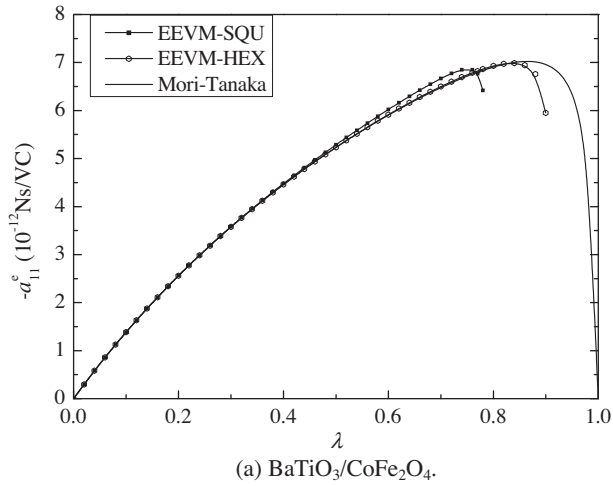
(a) BaTiO₃/CoFe₂O₄.

(b) Terfenol-D/BaTiO₃.

Fig. 2. Effective magnetoelectric coefficient ($a_{11}^e = a_{22}^e$) of the two-phase composites versus the fiber volume fraction: a comparison of the present series solutions (EEVM) for a square fiber array and a hexagonal fiber array, with the Mori-Tanaka estimation (Wang and Pan, 2007). (a) BaTiO₃/CoFe₂O₄; (b) Terfenol-D/BaTiO₃.

that the maximum of $|a_{11}^e|$ of the composite BaTiO₃/Terfenol-D ($a_{11}^e = -232.6 \times 10^{-12}$ Ns/VC at $\lambda = 0.88$) is at least one order larger than that of Terfenol-D/BaTiO₃. Therefore, besides the choice of the phases, the influence of the permutation can also be significant.

5.2.2. Three-phase composites

In Fig. 4, the effective magnetoelectric coefficient ($a_{11}^e = a_{22}^e$) of the three-phase composites ($(R_0/R)^2 = 1/2$) versus the total volume fraction of the fiber and interphase are depicted for a hexagonal fiber array. A comparison of six kinds of three-phase composites composed of CoFe₂O₄, BaTiO₃ and Terfenol-D in different permutations is also made. It is seen that the maximum of $|a_{11}^e|$ of the three-phase composite CoFe₂O₄/BaTiO₃/Terfenol-D ($a_{11}^e = -512.2 \times 10^{-12}$ Ns/VC at $\lambda = 0.86$) is the largest, which is much larger those of the two-phase composites composed of any two of CoFe₂O₄, BaTiO₃ and Terfenol-D. It is also interesting to note that, the composite Terfenol-D/BaTiO₃/CoFe₂O₄ has a positive a_{11}^e, while the other three-phase composites and all the two-phase composites have a negative one.

To reach the maximum of $|a_{11}^e|$ by optimizing the volume fraction of phases, the effective magnetoelectric coefficient ($a_{11}^e = a_{22}^e$) versus the total volume fraction λ and the square of radius ratio ($R_0/R)^2$ are depicted for a hexagonal fiber array, in Fig. 5(a) for three-phase composites CoFe₂O₄/BaTiO₃/Terfenol-D and in Fig. 5(b) for
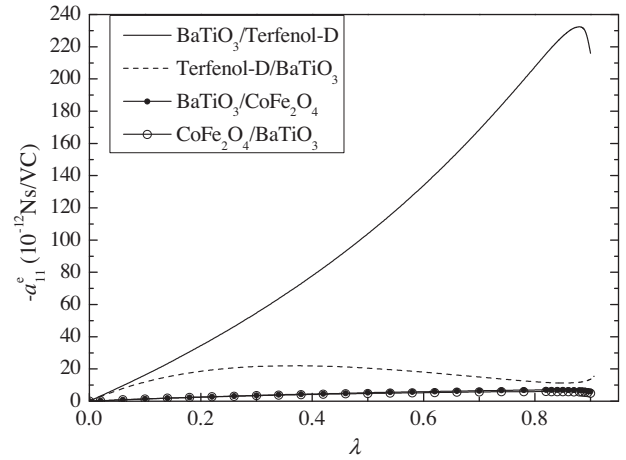

Fig. 3. Effective magnetoelectric coefficient ($a_{11}^e = a_{22}^e$) of the two-phase composites versus the fiber volume fraction for a hexagonal fiber array: a comparison of four kinds of two-phase composites.
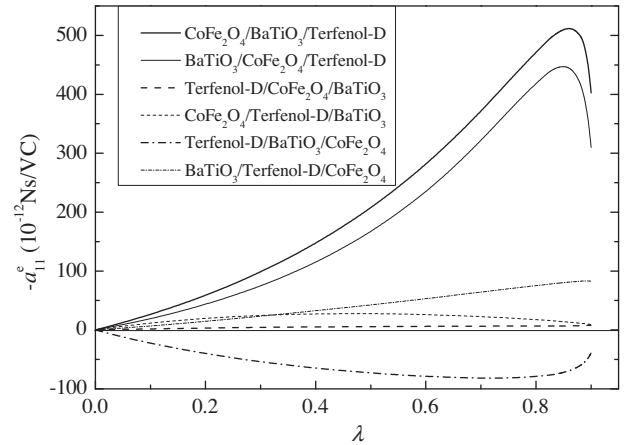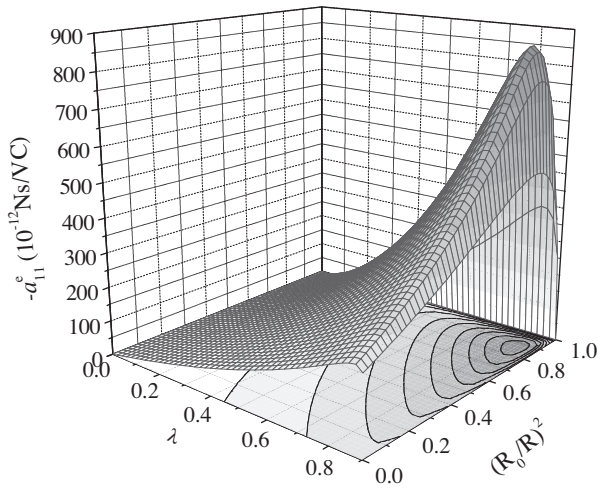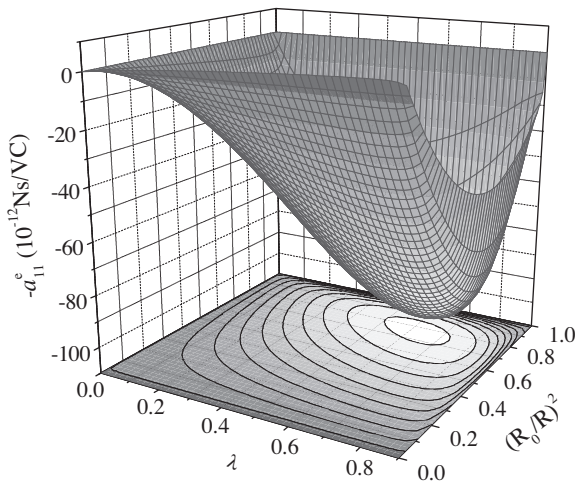

Fig. 4. Effective magnetoelectric coefficient ($a_{11}^e = a_{22}^e$) of the three-phase composites ($(R_0/R)^2 = 1/2$) versus the total volume fraction of the fiber and interphase for a hexagonal fiber array: a comparison of six kinds of three-phase composites composed of CoFe₂O₄, BaTiO₃ and Terfenol-D in different permutations.

Terfenol-D/BaTiO₃/CoFe₂O₄, respectively. It is seen from Fig. 5(a) that the maximum magnitude ($a_{11}^e = -862.3 \times 10^{-12}$ Ns/VC at $\lambda = 0.84$ and $(R_0/R)^2 = 0.88$) is about four times as large as that of the two-phase composite BaTiO₃/Terfenol-D in Fig. 3. In Fig. 5(b), there are two extrema of the magnitude with the variation of the phase volume fractions: a positive a_{11}^e (102.5×10^{-12} Ns/VC) is reached at $\lambda = 0.62$ and $(R_0/R)^2 = 0.78$; a negative a_{11}^e (-6.988×10^{-12} Ns/VC) is at $\lambda = 0.84$ and $(R_0/R)^2 = 0$. There exists a curve about λ and $(R_0/R)^2$ dividing the positive value area and the negative, at which a_{11}^e is zero. That is, at such values of λ and $(R_0/R)^2$ the overall magnetoelectric effect disappears though local magnetoelectric effect may still exist.

It is seen from Fig. 5(b) that the sign of the effective magnetoelectric coefficient of the composite Terfenol-D/BaTiO₃/CoFe₂O₄ changes according to the volume fraction of constituents. This phenomenon can be observed at both low and high fiber volume fractions, thus it can also be predicted by other methods. Motivated by this, a comparison of the present results with those predicted by generalized self-consistent model (GSCM) (derived from that for plane problems presented by Tong et al., 2008) is made, as shown in Fig. 6. It is seen that the present series solutions (EEVM) are in good agreement with the GSCM. Especially, at a relatively low fiber

(a) CoFe$_2$O$_4$/BaTiO$_3$/Terfenol-D

(b) Terfenol-D/BaTiO$_3$/CoFe$_2$O$_4$

Fig. 5. Effective magnetoelectric coefficient ($a_{11}^e = a_{22}^e$) versus the total fraction λ and the square of radius ratio $(R_0/R)^2$, for three-phase composites with a hexagonal fiber array. (a) CoFe$_2$O$_4$/BaTiO$_3$/Terfenol-D; (b) Terfenol-D/BaTiO$_3$/CoFe$_2$O$_4$.

volume faction ($\lambda = 0.3$) three curves almost totally coincide with each other. Interestingly, all curves meet at a point, where the effective magnetoelectric coefficient is zero. It is worth noting that for the anti-plane magnetoelectroelastic coupling problem under consideration, the results predicted by GSCM are equal to those predicted by Mori-Tanaka method.

5.3. Influence of the volume fraction and interphase on interfacial stresses

Another concern about magnetoelectroelastic composites is the strength. Stress concentration at the interface is one of the key factors which lead to the failure of composites. Especially, according to above discussions, the magnetoelectric coefficient reaches the extremum usually at a relatively high fiber volume fraction, where the interaction between fibers is strong. Thus the influence of the volume fraction and interphase on interfacial stresses will be investigated.

Now prescribe a macro-field condition: only the average stress over a unit cell $\langle \tau_{13} \rangle \neq 0$, while $\langle \tau_{23} \rangle$ as well as the other components of the average generalized stress are zero. The stress concentration factor (SCF) at the interface is defined as $\tau_{13}^{max}/\langle \tau_{13} \rangle$, where
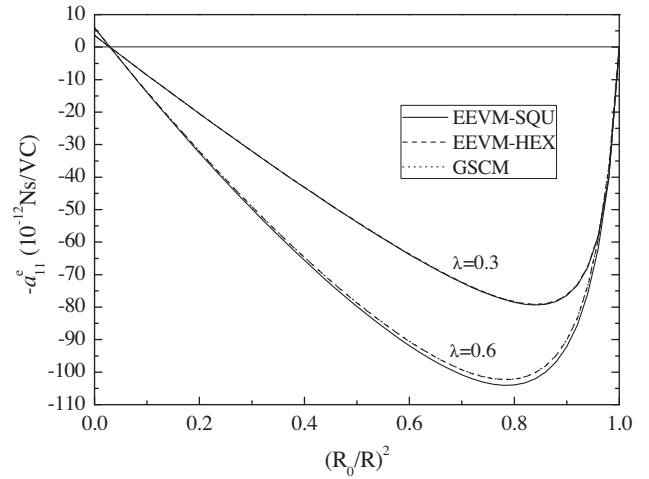

Fig. 6. Effective magnetoelectric coefficient ($a_{11}^e = a_{22}^e$) of the composite Terfenol-D/BaTiO$_3$/CoFe$_2$O$_4$ versus the square of radius ratio $(R_0/R)^2$ at a relatively low fiber volume fraction ($\lambda = 0.3$) and a relatively high fiber volume fraction ($\lambda = 0.6$), respectively: a comparison of the present series solutions (EEVM) for a square fiber array and a hexagonal fiber array, with the generalized self-consistent model (GSCM).

τ_{13}^{max} is the maximum stress τ_{13} at the interface between matrix and interphase. It is worth noting that for the cases of extremely soft fibers (holes) or extremely rigid fibers at an extremely low volume fraction, the SCF approaches 2.

In Fig. 7, the stress concentration factor (SCF) $\tau_{13}^{max}/\langle \tau_{13} \rangle$ of the three-phase composites mentioned in Fig. 5(a) and (b) (CoFe$_2$O$_4$/BaTiO$_3$/Terfenol-D and Terfenol-D/BaTiO$_3$/CoFe$_2$O$_4$, $R_0/R = 0.9$) versus the volume fraction λ is depicted. As for the influence of the volume fraction, it is seen from Fig. 7 that for the composite Terfenol-D/BaTiO$_3$/CoFe$_2$O$_4$ the SCF increases all along with the increase of the volume faction, whereas for the composite CoFe$_2$O$_4$/BaTiO$_3$/Terfenol-D it first decreases slightly then increases. As for the influence of the permutation of the phases, it is seen that at a relatively high volume fraction the SCF of the composite Terfenol-D/BaTiO$_3$/CoFe$_2$O$_4$ is much larger than that of the composite CoFe$_2$O$_4$/BaTiO$_3$/Terfenol-D. As for the influence of the fiber array, it is seen that at a relatively high volume fraction the SCF for a square fiber array is much larger than that for a hexagonal fiber array. Therefore, considering the strength of the composites, a hexagonal fiber array is more appropriate. For a hexagonal fiber array, the SCF of the composite CoFe$_2$O$_4$/BaTiO$_3$/Terfenol-D is always less than 1.6 even at an extremely high volume fraction $\lambda = 0.9$, and the SCF of the composite Terfenol-D/BaTiO$_3$/CoFe$_2$O$_4$ is less than 2 even when the volume fraction λ reaches 0.8.

In Fig. 8, the stress concentration factor (SCF) $\tau_{13}^{max}/\langle \tau_{13} \rangle$ of the two kinds of three-phase composites (CoFe$_2$O$_4$/BaTiO$_3$/Terfenol-D and Terfenol-D/BaTiO$_3$/CoFe$_2$O$_4$) versus the relative thickness $(R - R_0)/R$ of the interphase is depicted. It is seen from Fig. 8 that with the increase of $(R - R_0)/R$ the SCF of the composite CoFe$_2$O$_4$/BaTiO$_3$/Terfenol-D almost remains unchanged, whereas the SCF of the composite Terfenol-D/BaTiO$_3$/CoFe$_2$O$_4$ first decreases to near 1 then increases slightly.

5.4. Influence of the fiber distribution: distribution-induced anisotropy

The magnetoelectroelastic fiber composites discussed above as well as in the existing researches are almost all the ones with a square fiber array (Camacho-Montes et al., 2009; Espinosa-Almeyda et al., 2011; Kuo, 2011; Kuo and Pan, 2011) or a hexagonal fiber array (Espinosa-Almeyda et al., 2011) or a statistically even fiber distribution (Wang and Pan, 2007), whose effective magnetoelectric moduli are transversely isotropic, that is $a_{11}^e = a_{22}^e, a_{12}^e = a_{21}^e = 0$. For
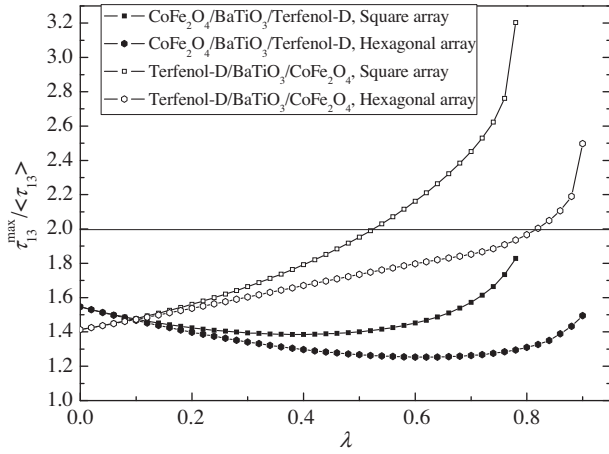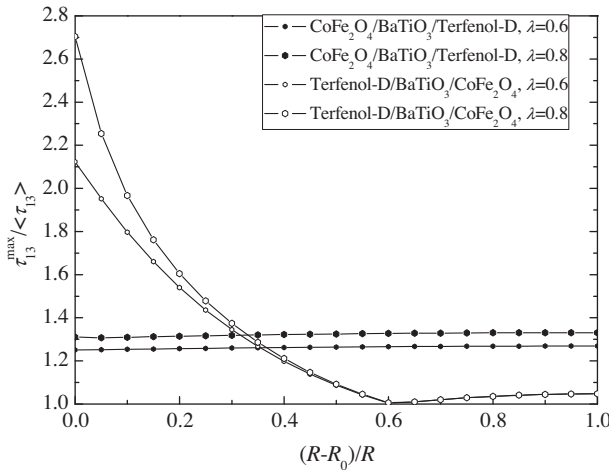
Fig. 7. Stress concentration factor $\tau_{13}^{\max}/\langle\tau_{13}\rangle$ at the interface of the three-phase composites (CoFe$_2$O$_4$/BaTiO$_3$/Terfenol-D and Terfenol-D/BaTiO$_3$/CoFe$_2$O$_4$, $R_0/R = 0.9$) versus the total volume fraction λ for a square fiber array and a hexagonal fiber array, respectively.

Fig. 8. Stress concentration factor $\tau_{13}^{\max}/\langle\tau_{13}\rangle$ at the interface of the three-phase composites (CoFe$_2$O$_4$/BaTiO$_3$/Terfenol-D and Terfenol-D/BaTiO$_3$/CoFe$_2$O$_4$) versus the relative thickness $(R - R_0)/R$ of the interphase, for a hexagonal fiber array at two volume fractions $\lambda = 0.6$ and $\lambda = 0.8$, respectively.

composites with a generally periodic array of fibers, the effective magnetoelectric moduli can be anisotropic, the overall magneto-electroelastic behaviors in two directions are coupled as stated in Eq. (26). To investigate such anisotropy induced by the general fiber arrays, a generally doubly periodic fiber array is parameterized with two parameters: side length ratio l_2/l_1 and relative staggered distance $\Delta l_1/l_1$ of the staggered rectangular unit cell, as shown in Fig. 9.

In Fig. 10(a) and (b), the effective magnetoelectric coefficients $(a_{11}^e, a_{22}^e, a_{12}^e)$ of the anisotropic three-phase composite (CoFe$_2$O$_4$/BaTiO$_3$/Terfenol-D, $R_0/R = 0.9$) versus the relative staggered distance $\Delta l_1/l_1$ are depicted for two cases: $l_2/l_1 = 1$, $\lambda = 0.7$ and $l_2/l_1 = \sqrt{3}/2, \lambda = 0.6$, respectively. It should be noted that the volume fraction keeps unchanged and only the fiber distribution varies with $\Delta l_1/l_1$ varying. The cases $l_2/l_1 = 1$, $\Delta l_1/l_1 = 0$ and $l_2/l_1 = \sqrt{3}/2$, $\Delta l_1/l_1 = 1/2$ are corresponding to two special symmetric arrays: square array and hexagonal array, respectively; while the cases $l_2/l_1 = 1$, $\Delta l_1/l_1 = 1/2$ and $l_2/l_1 = \sqrt{3}/2$, $\Delta l_1/l_1 = 0$ are corresponding to two general symmetric arrays: rhombic array and rectangular array, respectively. It is seen from Fig. 10(a) and
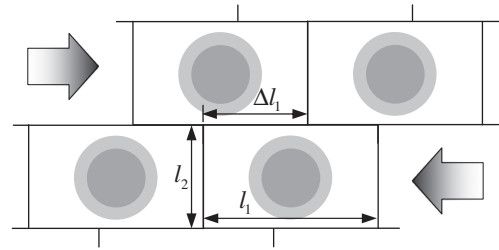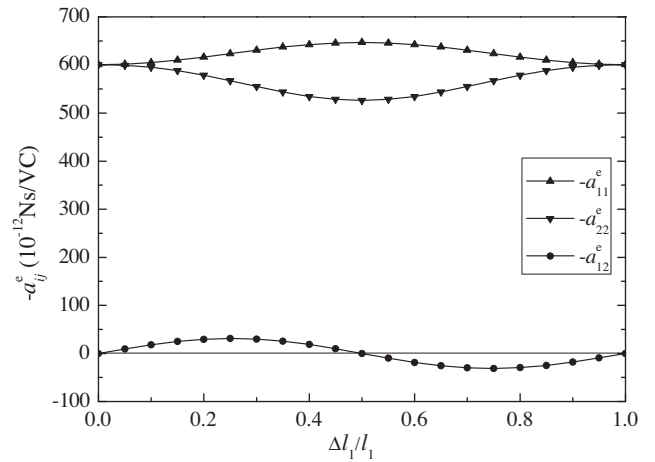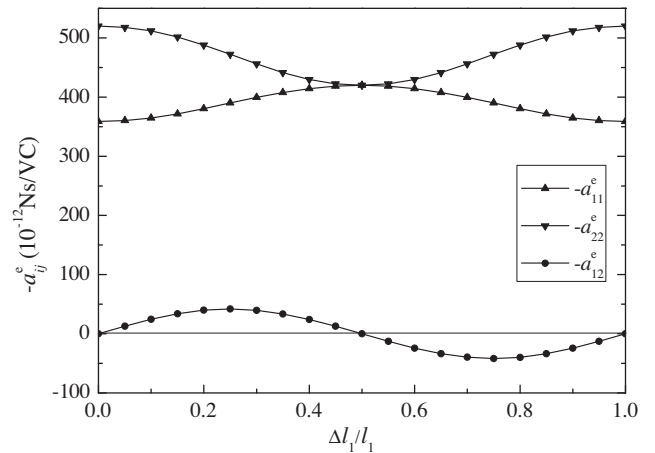

Fig. 9. A generally doubly periodic fiber array parameterized with two parameters: side length ratio l_2/l_1 and relative staggered distance $\Delta l_1/l_1$ of the staggered rectangular unit cell.

(a) Side length ratio $l_2/l_1 = 1$ and $\lambda = 0.7$

(b) Side length ratio $l_2/l_1 = \sqrt{3}/2$ and $\lambda = 0.6$

Fig. 10. Effective magnetoelectric coefficients $(a_{11}^e, a_{22}^e, a_{12}^e)$ of the anisotropic three-phase composite (CoFe$_2$O$_4$/BaTiO$_3$/Terfenol-D, $R_0/R = 0.9$) versus the relative staggered distance $\Delta l_1/l_1$. (a) Side length ratio $l_2/l_1 = 1$ and $\lambda = 0.7$; (b) side length ratio $l_2/l_1 = \sqrt{3}/2$ and $\lambda = 0.6$.

(b) that for above four symmetric arrays the coupling magneto-electric coefficient $a_{12}^e = 0$. With the transformation of the fiber distributions from the special symmetric arrays to the general symmetric arrays, a_{12}^e reaches its maximum magnitude in the middle of the process and its sign is variable, one of the main magnetoelectric coefficients (a_{11}^e and a_{22}^e) increases while another decreases. The maximum magnitude of the coupling magnetoelectric coefficient is about one order smaller than the magnitude of the main magnetoelectric coefficients.

6. Conclusions

With the aid of the matrix notation, the anti-plane magneto-electroelastic coupling problem is formulated as same as the anti-plane piezoelectric coupling problem. And then the eigenfunction expansion-variational method (EEVM) is extended to solve such a problem. Series solutions for the effective magnetoelectro-elastic moduli are presented, which are in a unified form for generally periodic fiber arrays, different unit cell shapes as well as different constituent properties, and are applicable for high volume fraction of fibers.

With the present series solution, it is found that the effective magnetoelectric coefficient of a two-phase composite may have two local extrema rather than only one extremum predicted by the Mori-Tanaka method. For a small fiber volume fraction, the results by the present method are in agreement with those by the Mori-Tanaka method. However, for a large volume fraction, the Mori-Tanaka method fails to predict the correct results and the present method is required. By optimizing the volume fraction, permutation and the choice of the constituent phases, the maximum magnitude of the effective magnetoelectric coefficient of a three-phase composite can be much larger than that of any of the two-phase composites, and the sign of the magnetoelectric coefficient can be changed, which is not observed in a two-phase composite.

For composites with a generally periodic array of fibers, the effective magnetoelectric moduli can be anisotropic. There exist two coupling magnetoelectric coefficients besides the two main coefficients. The maximum magnitude of the coupling magneto-electric coefficient is about one order smaller than the magnitude of the main magnetoelectric coefficients.

Acknowledgements

References

Benveniste, Y., 1995. Magnetoelectric effect in fibrous composites with piezoelectric and piezomagnetic phases. Phys. Rev. B 51, 16424–16427.

Boyd IV, J.G., Lagoudas, D.C., Seo, C.S., 2003. Arrays of micro-electrodes and electromagnets for processing of electromagneto-elastic multifunctional composite materials. In: Varadan, V.K., Kish, L.B. (Eds.), Smart Structures and Materials 2003: Smart Electronics MEMS, BioMEMS, and Nanotechnology. San Diego, CA, pp. 268–277.

Camacho-Montes, H., Sabina, F.J., Bravo-Castillero, J., Guinovart-Díaz, R., Rodríguez-Ramos, R., 2009. Magnetoelectric coupling and cross-property connections in a square array of a binary composite. Int. J. Eng. Sci. 47, 294–312.

Dinzart, F., Sabar, H., 2011. Magneto-electro-elastic coated inclusion problem and its application to magnetic-piezoelectric composite materials. Int. J. Solids Struct. 48, 2393–2401.

Eerenstein, W., Mathur, N.D., Scott, J.F., 2006. Multiferroic and magnetoelectric materials. Nature 442, 759–765.

Espinosa-Almeyda, Y., López-Realpozo, J.C., Rodríguez-Ramos, R., Bravo-Castillero, J., Guinovart-Díaz, R., Camacho-Montes, H., et al., 2011. Effects of interface contacts on the magneto electro-elastic coupling for fiber reinforced composites. Int. J. Solids Struct. 48, 1525–1533.

Huang, J.H., Kuo, W.S., 1997. The analysis of piezoelectric/piezomagnetic composite materials containing ellipsoidal inclusions. J. Appl. Phys. 81, 1378–1385.

Kuo, H.Y., 2011. Multicoated elliptic fibrous composites of piezoelectric and piezomagnetic phases. Int. J. Eng. Sci. 49, 561–575.

Kuo, H.Y., Pan, E., 2011. Effective magnetoelectric effect in multicoated circular fibrous multiferroic composites. J. Appl. Phys. 109, 104901.

Lee, J., Boyd IV, J.G., Lagoudas, D.C., 2005. Effective properties of three-phase electro-magneto-elastic composites. Int. J. Eng. Sci. 43, 790–825.

Li, J.Y., 2000. Magnetoelectroelastic multi-inclusion and inhomogeneity problems and their applications in composite materials. Int. J. Eng. Sci. 38, 1993–2011.

Li, J.Y., Dunn, M.L., 1998. Micromechanics of magnetoelectroelastic composite materials: average fields and effective behavior. J. Intell. Mater. Syst. Struct. 9, 404–416.

Ma, J., Hu, J.M., Li, Z., Nan, C.W., 2011. Recent progress in multiferroic magnetoelectric composites: from bulk to thin films. Adv. Mater. 23, 1062–1087.

Nan, C.W., 1994. Magnetoelectric effect in composites of piezoelectric and piezomagnetic phases. Phys. Rev. B 50, 6082–6088.

Nan, C.W., Bichurin, M.I., Dong, S.X., Viehland, D., Srinivasan, G., 2008. Multiferroic magnetoelectric composites: historical perspective, status, and future directions. J. Appl. Phys. 103, 031101.

Nemat-Nasser, S., Hori, M., 1999. Micromechanics: Overall Properties of Heterogeneous Materials. Elsevier, Netherlands.

Pyu, J., Priya, S., Uchino, K., Kim, H.E., 2002. Magnetoelectric effect in composites of magnetostrictive and piezoelectric materials. J. Electroceram. 8, 107–119.

Ramesh, R., Spaldin, N.A., 2007. Multiferroics: progress and prospects in thin films. Nat. Mater. 6, 21–29.

Shi, Z., Nan, C.W., Zhang, J., Cai, N., Li, J.F., 2005. Magnetoelectric effect of Pb(Zr, Ti)O3 rod arrays in a (Tb, Dy)Fe2/epoxy medium. Appl. Phys. Lett. 87, 012503.

Spaldin, N.A., Fiebig, M., 2005. The renaissance of magnetoelectric multiferroics. Science 309, 391–392.

Srinivas, S., Li, J.Y., 2005. The effective magnetoelectric coefficients of polycrystalline multiferroic composites. Acta Mater. 53, 4142–4153.

Srinivas, S., Li, J.Y., Zhou, Y.C., Soh, A.K., 2006. The effective magnetoelectroelastic moduli of matrix-based multiferroic composites. J. Appl. Phys. 99, 043905.

Srinivasan, G., 2010. Magnetoelectric composites. Annu. Rev. Mater. Res. 40, 153–178.

Sun, W., Lin, F., Hu, X., 2001. Computer-aided design and modeling of composite unit cells. Compos. Sci. Technol. 61, 289–299.

Tong, Z.H., Lo, S.H., Jiang, C.P., Cheung, Y.K., 2008. An exact solution for the three-phase thermo-electro-magneto-elastic cylinder model and its application to piezoelectric-magnetic fiber composites. Int. J. Solids Struct. 45, 5205–5219.

Van Run, A.M.J.G., Terrell, D.R., Scholing, J.H., 1974. An in situ grown eutectic magnetoelectric composite materials. Part 2: physical properties. J. Mater. Sci. 9, 1710–1714.

Van Suchtelen, J., 1972. Product properties: a new application of composite materials. Philips Res. Rep. 27, 28–37.

Wang, X., Pan, E., 2007. Magnetoelectric effects in multiferroic fibrous composite with imperfect interface. Phys. Rev. B 76, 214107.

Wu, T.L., Huang, J.H., 2000. Closed-form solutions for the magnetoelectric coupling coefficients in fibrous composites with piezoelectric and piezomagnetic phases. Int. J. Solids Struct. 37, 2981–3009.

Yan, P., Jiang, C.P., Song, F., 2011. An eigenfunction expansion-variational method for the anti-plane electroelastic behavior of three-phase fiber composites. Mech. Mater. 43, 586–597.

Zhang, Z.K., Soh, A.K., 2005. Micromechanics predictions of the effective moduli of magnetoelectroelastic composite materials. Eur. J. Mech. A. Solids 24, 1054–1067.

Zheng, H., Wang, J., Lofland, S.E., Ma, Z., Mohaddes-Ardabili, L., Zhao, T., 2004. Multiferroic BaTiO$_3$–CoFe$_2$O$_4$ nanostructure. Science 303, 661–663.

Zohdi, T.I., 2008. On the computation of the coupled thermo-electromagnetic response of continua with particulate microstructure. Int. J. Numer. Methods Eng. 76, 1250–1279.